Materials Research. 2023; 26:e20220077
DOI: https://doi.org/10.1590/1980-5373-MR-2022-0077

The Morphology of al Droplet in an Ultrasonic Oscillation Field: Kinetic and Equilibrium Thermodynamic Analysis

***Wendi Li*[a,b], *Yuxin Liang*[a], *Yao Yang*[a], *Bangsheng Li*[a,b,c], *Jicai Feng*[a,b,*]**

[a]*Harbin Institute of Technology, School of Materials Science and Engineering, 150001, Harbin, China.*
[b]*Harbin Institute of Technology, State Key Laboratory of Advanced Welding and Joining, 150001, Harbin, China.*
[c]*Harbin Institute of Technology, National Key Laboratory for Precision Hot Processing of Metals, 150001, Harbin, China.*

Received: February 13, 2022; Revised: October 07, 2022; Accepted: November 16, 2022

Wetting of metal droplet on the solid substrate is a fundamental phenomenon which is applicable to the surface chemistry. When an oscillation field is included in the wetting condition, the wetting process shows significant advancing and receding behaviors. Also, the use of ultrasonic oscillation field is promising in welding. However, some odd morphologies led by the ultrasonic-treatment have shown wetting kinetics which have not been fully investigated.

The high frequency ultrasonic vibration brings hysteresis to the contact angle, whose extra energy is attributed by the oscillation field. The ultrasonic wetting process is excited by the 20 kHz frequency periodic oscillation, during which droplet is swaying cyclically. However, after capturing the transformation of droplet morphologies, it is found that the frequency of each swaying cycle is identified to be 180 ms. Theoretical investigations have also quantitively proved that the energy for the contact angle decrease origins from the ultrasonic field, and the wettability is in a great enhancement. Thermal and kinetic effects of ultrasonic are investigated by making theoretical calculations, the 20 kHz ultrasonic field lasting for 5 seconds. Thermodynamics, vibrational mechanics, and interfacial phenomena affect the sonochemistry of wetting.

Keywords: *Ultrasonic, Al/SiC wetting, Contact angle hysteresis, Thermodynamics.*

1. Introduction

Wetting phenomenon is a fundamental issue, which is generally indicated as distribution of a liquid droplet on a solid surface[1,2]. Along with light interaction, and friction phenomenon, they all play very significant roles in the practical applications of surface chemistry. In the area of additive manufacturing, considerable works such as fast-atom-beam irradiation, 3D printing, and chemical etching[3-5] are all deeply related with the static or dynamic wetting phenomena. And for microfluidic area, it is also a feasible idea to manipulate the liquid-solid contact line movement utilizing the fluid mechanics, already been used for mixing[6], pumping[7,8], and particle manipulation[9]. The kinetic control of wetting liquid has long been a cutting edge. However, researchers still can not break through plenty of difficulties in the manipulation of Al droplets at high temperatures[10]. Due to the strong reactivity between Al and solid substrate, the routine flowing path of metal liquid is always obstructed, when placing Al on SiC, Si_4N_3, and Al_2O_3 surfaces at elevated holding temperatures[11-13].

Recently, the usage of ultrasonic-treatment has shown dissimilar spreading characteristics, in the wetting process of water/substrate[14]. The traditional ultrasonic-treatment is considered to be clean and efficient[15]. Now being experimentally proved, the ultrasonic-assisted methods are capable of manipulating fluids with normally flowabilities, through inputting acoustic waves with several levels of frequencies[16]. Till now, phenomena from manufacturing process are already used for the verification of ultrasonic effect on wettability improvement[17-20]. In addition, there are some essential factors like acoustic cavitation, streaming effect which are uneasy to predict in ultrasonic wetting.

How to improve the wettability is still a major problem in desperate need of a better solution. However, the manipulation method is far less efficient in some industries in need of even more ideal wettability. In many metallic, metal/ceramic systems, wetting are vital issues concerned by microelectronics, aerospace, and so forth. Applications of high-temperature brazing also favor materials with a lower viscosity and a higher surface tension, therefore, the reliability of a brazing joint has better performance and quality of alloy usage. Intrinsically speaking, brazing process of an Al-based alloy is always accompanied with physical changes and chemical reactions, making matters more complicated[21,22].

Wettability of solder droplet can be enhanced in some external conditions, like an electric/electromagnetic or an infrared laser field[23]. A significant evidence of wettability enhancement is the contact angles being decreased. Compared with infrared laser,

*e-mail: hit_fengjc@163.com

electrical current or even plasma jet which injects the direct flow of energy into wetting, the energy induced by ultrasonic excitation is uncontinual and fluctuant. Electrowetting has already got adequate theories, like the Young-Lippmann equation in electrostatic model, which well explains contact angle variation happened in electrolyte droplets[24,25].

Yeo elucidates the mechanism of static contact angle change using asymptotic analysis[26], The contour outline of droplet is usually asymmetrical, which associated with hysteresis[27,28]. Nevertheless, hysteresis brings tiny instability for wetting behaviors of a droplets, it might shift droplet motion into a swaying manner. The forced oscillation can also change the wettability of liquid droplet on a flat surface as was shown by Chaudhury, the experiment was performed with a water drop and in laboratory settings[29], and later on it becomes a pilot project for lateral migration of oscillatory flows[30-32]. Similarly, researchers observe the existence of wettability oscillation of metal filler materials[33], according to the phenomena, metal droplets in soldering are forced to spread on substrate materials which were hard to weld, with the same mechanism, vibrating squeegee, vibratory arc surfacing and ultrasonic soldering[34,35]. Till now, research have not reached a consensus on the driven force of high-temperature molten drop oscillations, certain laws of wetting front instability[36,37], and contact line mobility in vibration systems remain unclear[38].

In this paper, some calculations were made for Al/SiC ultrasonic wetting from the energy viewpoints. The calculation results were confirmed by following experiments of the wetting process. Besides, the relevance between Al/SiC wettability and the amount of additional energy were built, basing on fundamental acoustic theories. Characteristics of contact angle (CA, θ) were quantitatively estimated, which were finally demonstrated in detail by some theoretical equations.

2. Experimental

The apparatus includes a heater, an observation device, a gas supply and an ultrasonic device. The main equipment is named monitoring system for in-situ solder spreading tests, made by KYKY Co., Ltd. The ultrasonic device is assembled together by four parts, an intelligent generator (TJS-3000, V6.0 Hangzhou China), a steady 300 W power amplifier, an ultrasonic horn and a sliding platform. The device outputs continuous-wave with frequency f (f = 20 kHz) during excitation. The laser doppler vibrometer apparatus (*LDV*) is an inserted auxiliary for measuring amplitudes on the center of substrate surface (a_s). The amplitude of the ultrasonic wave peaks at 6.338 μm. The schematic of experimental apparatus is shown in Figure 1.

The high-speed digital camera in use is the brand Phantom V12.1, with a maximum resolution 1 200×800 pixels (WXGA). Set the camera to 20 000 frames per second when capturing motion of droplet, in step with the transformation of periodic ultrasonic wave, thus more instant details of spreading kinetics can be included in snapshots. The backlight serves as an additional facility, using collimated light to guarantee the quality of videos. Being overlooked from the top, Figure 2 shows relative spatial positions between backlight, the wetting sample, and the camera.

As filler material, aluminum is commonly used in high temperature vacuum brazing, utilizing its good fluidity. The property data of Al and SiC are listed in Table 1. The Al and SiC act as the test piece and the substrate respectively. Each Al piece weighs 0.1 gram, which has a rounded shape.

Prior to spreading tests, substrates were cleaned ultrasonically in acetone for 10 min. After drying, a substrate sample was first placed into the furnace pinning on the inner platform with a homocentric squares mold, then placed one piece of Al on the substrate (after caustic washed). Inside the furnace, pressure was limited to less than 5×10^{-3} Pa with a molecular pump, and then the heating of the test material of Al/SiC was started. The substrate sheet had dimensions of 2.5 mm × 2.5 mm × 1 mm and was single-side polished. The sheet and the Al piece were heated to the predetermined temperature of 900 °C with a constant heating rate of 10 °C/min. And a Platinum-Rhodium thermocouple wire was used

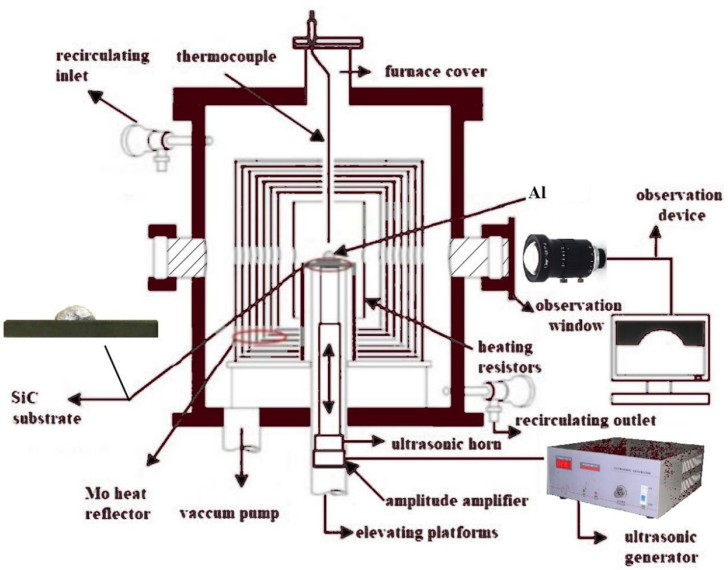

Figure 1. Schematic diagram of the ultrasonic device for wetting experiments.

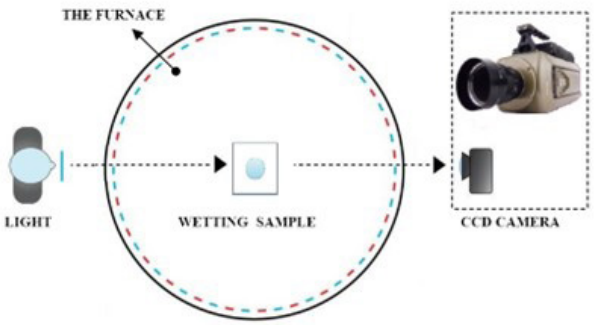

Figure 2. Schematic of photographic facilities using in wetting experiments, what inside the circle with dash line is actually invisible viewing from the top.

Table 1. Features of the metal and substrate samples.

Test piece			Substrate
99.999%-purity Al, refined			SiC, sintered
Properties	Bulk density ρ	2 320 kg/m^3	3 150 kg/m^3
	Acoustic velocity c	4 640 m/s	4 800 m/s
	Mass m	0.1×10^{-3} kg	3.3×10^{-3} kg
	Melting point T	660 °C	2 827 °C
	Allowable temperature T_a	1 600 °C	2 327 °C

to manipulate heating progress. After switching on the ultrasonic generator, the ultrasonic vibration was propagated into the wetting sample through the tool head on the bottom. When the ultrasonic vibration system was operating, ultrasonic waves had the rated input power of 300 W, and the fixed frequency of 20 kHz. The entire process was synchronously recorded by CCD camera until the test ended, then images were stored for further post-processing. The video and image analysis were done with the PhotoLine V17.54 software.

3. Results and Discussions

3.1. Kinetics of wetting with ultrasonic

When there is no additional ultrasonic fields, interfacial reaction between liquid and solid dominates the dynamic wettability of Al/SiC. Shen et. al already made the predictions for the reactive wetting performances[39]. When with no ultrasonic, trends of investigation are similar to those from the measurement from ultrasonic demonstrated by Figure 3.

During the non-ultrasonic spreading processes, the pinning contact lines have been inert in the wetting field for 1 hour. At the ambient temperature of 900 °C, the projection length of solid-liquid contact line is indicated to reach 3.48 mm. Hence, the moving droplet has a cessation of spreading. The main reason for the bad Al/SiC wettabilities is supposed to be: solid/liquid contact line is not activated on the substrate surface with over-high surface energy. However, the contact line repeatedly sets its position at various stages of ultrasonic oscillation. The energy input makes energy enough to the activation of liquid's mobility. The phenomenon at the wetting front is made clear by observing that front. In the ultrasonic wetting field, the wetting front shows the variation which is caused by high frequency contact angle hysteresis. This pattern of pendular oscillating is now known as "swaying mode" hysteresis. In Figure 3b, the imagery with Al/SiC ultrasonic wetting screenshots is illustrated. Each two of the images in Figure 3a have the interval of 10 ms. When the oscillation mode is just like rolling either towards left or towards right.

Except that there is no hysteresis (x_{LL}–x_{UL} = x_{LR}–x_{UR}), there are two different kinds of situations. The first one appears when Abs(x_{LL}–x_{UL}) < Abs(x_{LR}–x_{UR}), (Abs( ) is short for absolute value), as is shown in the left side of the schematic, Figure 3b. The hysteresis of CA brings molten droplet with a horizon velocity from the lower-left to the upper-right. In this situation, the advancing angle is higher than the receding angle, on the left the value is close to 90 degree. If Abs(x_{LL}–x_{UL}) > Abs(x_{LR}–x_{UR}), it turns to be the other situation. As demonstrated by the rightward configuration, the hysteresis opposes to the other part. Through the above analysis, the contact angle hysteresis is strongly affected by the differential value between advancing/receding angles.

3.2. Contact angles when at equilibrium

Alike Figure 3, there is the type of swaying mode when in motion during droplet's ultrasonic spreading process. The vertex of its outline is repeating a left-most to right-most moving action, while the upper body tends to rotate

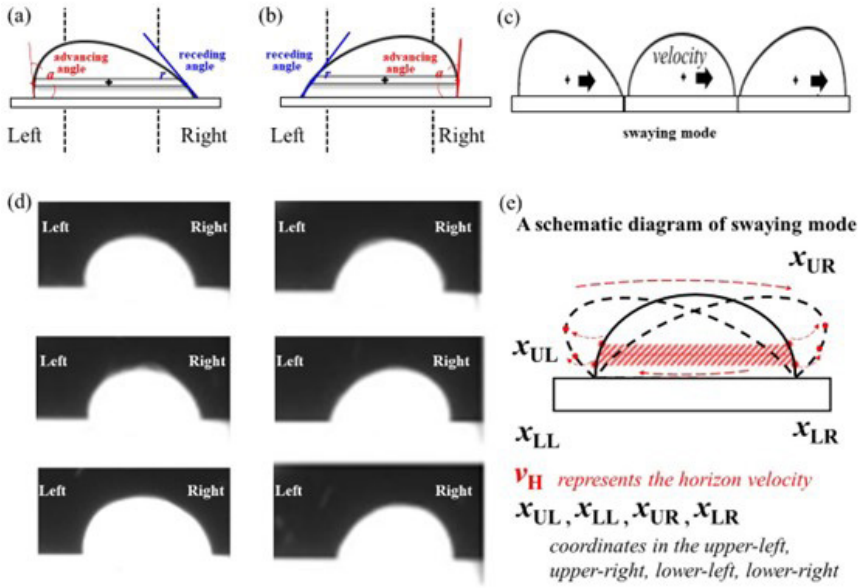

Figure 3. Imagery examples of two types of contact angle hysteresis in the kinetic studies of Al/SiC wetting under the excitation of 20 kHz ultrasonic wave. After showing advancing/receding angle alternatively (a) on the left or (b) on the right side, (c) a schematic of the mechanism of hysteresis, (d) Images with contact angle hysteresis phenomenon, (e) an illustration of changing the coordinate of both sides by the ultrasonic treatment.

from left to right side horizontally. The solid-vapor contact line is not moving in a regular way that is the circular relaxation. Instants in the middle of every single period acted as the temporal cessation of swaying, with a hint of the metastable condition of wetting. Based on assumptions of dynamic wetting, the extension in wetted area might emerge among different metastable wetting states. And in ultrasonic wetting field, the metastable state shows plenty of equilibrium contact angles (CA, θ).

Finally spreading behaviors terminate, the values are still confined to the radian range (0.3π, 0.5π) for θ_f. The variation of θ_f is demonstrated by a chart in Figure 4, and the significant decreasing trend of CA indicates that ultrasonic excitation has promoted the spreading degree of molten aluminum on the substrate.

As is shown from Figure 4, the equilibrium contact angle suddenly decreases from 93.0 ° to 89.86 ° during the first 0.4 s, that means the change of wetting situation which starts from the non-wetting situation and turns into the partially wetting simulation. In the transformation process, the thickness of the oxide layer around the droplet is cutting down. It can be deduced that ultrasonic waves brought the effect of ultrasonic cavitation. According to the viewpoint of Xu, ultrasonic cavitation can elevate the gaseous pressure inside wetting furnace[40]. Therefore, the broken process of Al to the Al_2O_3 oxidation will be elevated. Ultrasonic cavitation has a promoting effect to increase the wettability by removing oxide films.

Around the triple points at wetting fronts of the Al/SiC system, we value CA as the angles between tangent lines drawn by both liquid-vapor and solid-liquid phases. As can be seen in Figure 5, twenty-five images by CCD camera are listed matching with CA values in Figure 4. Each snapshot casts the droplet body into the

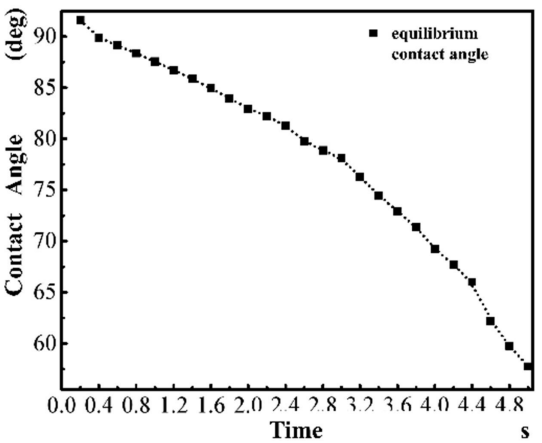

Figure 4. A chart of equilibrium contact angles during ultrasonic wetting period, CA values are measured from wetting snapshots in every single 0.2 s

shadow of the two-dimensional images, which makes CA able to be valued in a cross-section plane. By analyzing the swaying mode droplet motion inside an ultrasonic wetting process, the significant differences are found indeed existing between CAs on left and right, as are shown in Figure 3b.

Under such case, CAs represent advancing angles when in droplet's advancing fronts and are bigger than receding ones in other fronts. CA is investigated within initial time period (wetting in 0 s - 0.6 s ultrasonic period) with hysteresis, so error bars are used for identification in Figure 6.

Since the ultrasonic body force loading on aluminium droplet is rigid and knowable, the frequency of the period

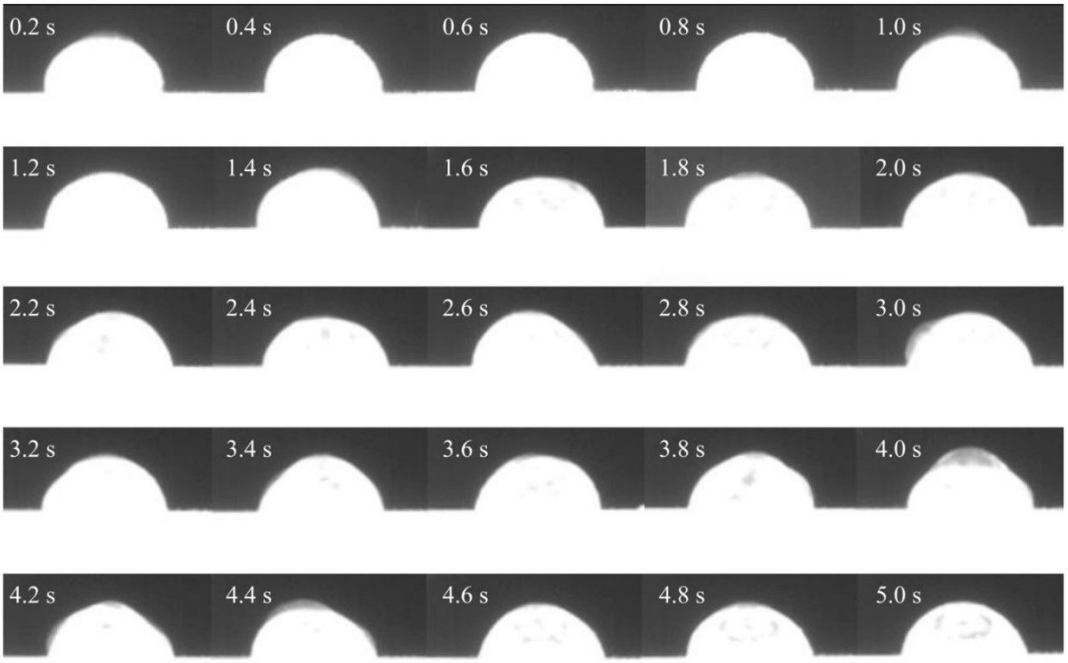

Figure 5. A series of wetting snapshots of Al/SiC contacts under a 20 kHz sustained ultrasonic vibration, snapshots are picked once every 0.2 s, which shows the typical morphologies of an Al droplet in equilibrium states during ultrasonic wetting.

for CA hysteresis is generally supposed to be a constant. Because of the irregular propagation path of acoustical wave at each time moment, the introduction of the external ultrasonic energy is in one-way mode. That is what being described in Figure 6. So the density of surface energy γ_{lv} in each part of the liquid aluminum is heterogeneous. For the incompressible liquid, the energetic equation meets Equation 1:

$$dU = TdS + \gamma_{lv} dA_{surface} \tag{1}$$

when the aluminum droplet has the potential to increase $A_{surface}$, Equation 1 is integrated into Equation 2.

$$\frac{\Delta U}{\gamma_{lv}} = \left(1 - cos\theta_t\right)\left(\frac{2V}{h} - \frac{\pi h^2}{3}\right) - \pi\left(h_0^2 - h^2\right) \tag{2}$$

In this sense, the ultrasonic vibration and contact angle hysteresis behave in the similar way. The droplet shape oscillation has its periodic routine. Here, we depict several rows of evolutive graphics, in order to identify the oscillation period. Just 10 ms later, there is no CA hysteresis. Judging from Figure 7, the end of a single circulation appears at 190 ms when droplet's wetting angle is also of no hysteresis. The frequency of CA hysteresis is 5.55 Hz.

From CA charts in the beginning and ending stages of ultrasonic wetting, the droplet shapes at different times are easily acknowledged, and the corresponding contour lines are fitted. The basic premise of those supposes is that droplet volume stays fixed. It is assumed that the evaluated variation of item E_k mainly depicts the height, contact line diameter, and the base area. E_k indicates the kinetic energy

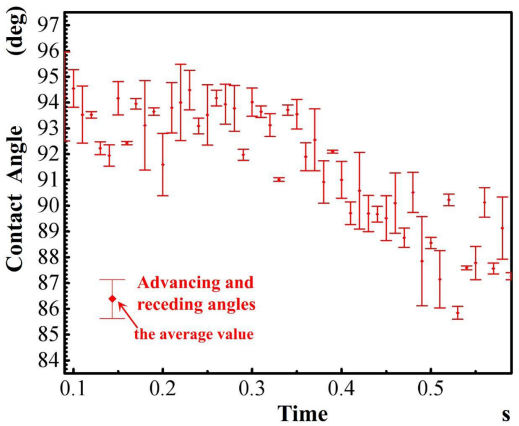

Figure 6. The CA variation from 0 s to 0.6 s during the ultrasonic exciting period, each two adjacent data share with 0.01 s time interval. Error bars are attached to ultrasonical CA on according to the "swaying mode".

for droplet in an ultrasonic field. As periodic oscillation is activated by the propagation of ultrasonic wave, changing kinetic energies are the relevant influencing factor for CA hysteresis measurements. So the variation of instantaneous horizontal velocity, v_H, seeing Figure 3b, is the pre-requisite for causing CA hysteresis. In the meantime, the position of moving droplet's centroid is continually fluctuating, being accompanied by ultrasonic oscillation. Further, the height of droplet is averaged. By dividing into *n* layers on average, mechanical energy increment is calculated by the instant velocity of droplet. The droplet contour is cut into *n* pieces,

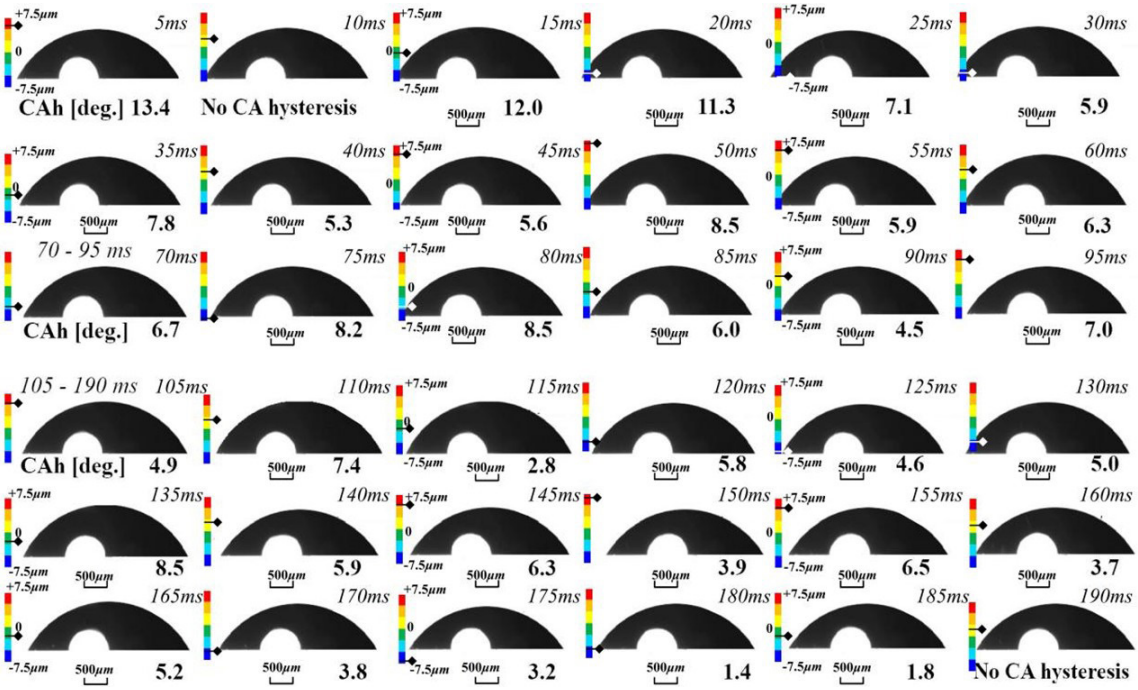

Figure 7. Images and screenshots of dynamic behaviors of Al/SiC wetting, the ultrasonic was primally activated, snapshots of dynamic CA hysteresis within time ranges 5 ms - 60 ms, 70 ms - 95 ms, and 105 ms - 190 ms.

as is demonstrated by the time-variant images in Figure 5. It is assumed that contribution of ultrasonic wetting energy is related to the kinetic item E_k in Equation 3, to be convenient for further calculations.

$$E_k = \frac{1}{2}\rho_l (h/n)\Sigma(v_1^2 A_i) \left(i = 1...n, A_i = k_i A_1, A_1 \approx A_{interface}\right) \quad (3)$$

If considering laws of energy, exhibition of the difference between the advancing and receding CA was due to metastable energy states. Droplet in oscillating path was indisputably facing energy barriers embodied in hysteresis behaviors. If with no sufficient energy to overcome the instantaneously finite energy barrier, oscillations in vibration was ruled by complex metastable energy states, thus liquid contour was in asymmetrical relaxation. However, when in equilibrium mode, the arrival of equilibrium energy states indicated that droplet had overcome the former barrier and drifted into the following energy states. Among these energy barriers, there must be some local global energy minimums in need of investigations.

3.3. Droplet spreading in thermo-kinetics

It is well known as a fact that droplet on an ultrasonic vibrating substrate can extend outwards during its wetting process. Thermo-kinetic models are needed, so as to evaluate dynamic spreading characteristics and thermodynamic changes at the same time in one step.

According to thermo-kinetics, the drop's spreading obeys the law of thermodynamics, and there are variable qualities like r, $A_{interface}$, $A_{surface}$, contact angle θ, and t in the dynamic wetting process. As is clearly illustrated by schematic

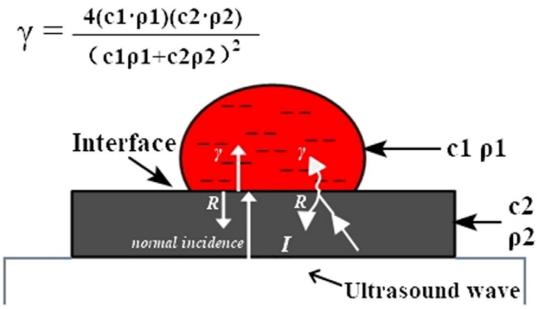

Figure 8. Schematic of the energy flow propagating in Al/SiC wetting system.

presented on Figure 8, the variables $A_{interface}$, $A_{surface}$, θ are both time-dependent and being mutually relevant. θ(t) relates with two area characteristics $A_{interface}(t)$ and $A_{surface}(t)$, both are functioned by time. Here, Equation 4 and 5 demonstrate the geometric relationships.

$$A_{surface}(t) = 2\pi C^2 \left(1-\cos\theta(t)\right)^{-1/3} \left(2+\cos\theta(t)\right)^{-2/3}, C = \sqrt[3]{3V/\pi} \quad (4)$$

$$A_{interface}(t) = \pi C^2 \left(1+\cos\theta(t)\right)\left(1-\cos\theta(t)\right)^{-1/3} \left(2+\cos\theta(t)\right)^{-2/3}, C = \sqrt[3]{3V/\pi} \quad (5)$$

Based on thermodynamic equations, the thermo-kinetic equation for ultrasonic wetting is like Equation 6.

$$P_{Ultrasonic-Force} \cdot A_{interface}(t) = W + Q = \Delta U = \gamma_{lv} \cdot A_{surface}(t)cos\theta + \frac{1}{2}\rho(h/n)\Sigma(v_i^2 A_i) \quad (6)$$
$$(A_i = k_i A_1, i = 1...n, A_1 = A_{interface}(t))$$

In the above equation, ΔU is the increase in internal energy while W is the ultrasonic work in the droplet/substrate system. At any arbitrary moment, I, II, ···, IV (t_1<t_{VI}), wetting characteristics are in compliance with the potential energy, and the kinetic energy. There must have the calculation of ultrasonic energy which is pouring into the solder. When the additional energies from the 300 W ultrasonic fields are spreading into the droplet, they meet an advanced quantitative evaluation. As is depicted in Figure 8, a steady energy flow enters into SiC then propagates towards molten droplet sample above. Wave propagates to the melt perpendicularly, but it meets incidence (coefficient *I*), reflection (*R*), refraction simultaneously, and the relationship expresses as $I = R+\gamma$.

The refraction coefficient of acoustic pressure depends on acoustic impedance Z ($Z = \rho c$, the density ρ and the acoustic speed c). It is originally measured by OFV apparatus that the amplitude on substrate surface suffering harmonic vibration peaks at 6.338 μm (a_{solid}). During the whole vibration period, root mean square amplitude $a_{solid/rms}$ equals to $(\sqrt{2}/2)$ $a_{solid/max}$. Further calculations of a_{solid} are based on Equation 7 (wave equation), and Equation 8 (the equation of motion):

$$a_{solid} = a_{solid/max} sin(2\pi \cdot f \cdot t + \Phi) \quad (7)$$

$$da_{solid} = u_{solid} dt \quad (8)$$

Velocities of vibrational mass points on solid surface u_s can be defined with density ρ_{solid}, acoustic pressure p_{solid}, and time t, seeing Equation 9.

$$\rho_{solid} du_{solid} = -gradp_{solid} dt \quad (9)$$

Similarly, in Equation 10, p_{liquid} is used to represent the acoustic pressure on bottom surface with ultrasound waves propagating into the droplet.

$$p_{liquid} = \gamma\left(2\pi \cdot f \cdot \rho_{liquid} \cdot c_{liquid} \cdot a_{solid/max}\right) \quad (10)$$

Acoustic wave intensity relates to both pressure and impedance ($I = p_{liquid}^2/\rho_{liquid}c_{liquid}$). The value dW/dA is solvable with Equations 11 and 12. It represents the work amount made by ultrasonic on a unit area of interface A. In this paper, $A_{interface}$ demonstrates the area of solid-liquid interface.

$$(\rho_{liquid} c_{liquid}) dW = (p_{liquid}^2 t) dA \quad (11)$$

$$P_{adsorpt} = p_{liquid}^2 A_{interface} / (\rho_{liquid} c_{liquid}) \quad (12)$$

Since only conservative forces emerge in cycles of mechanical vibration, the calculation of cumulative work for droplet takes attenuation into consideration. $\triangle W$ equals to the amount of attenuation, sustainably promoted when extending ultrasonic time duration. Providing that ultrasound suffers losses after propagating into molten solder, nonlinear effect of this acoustic attenuation reduces the amplitude of wave.

The fully enclosed wetting environment loses part of its energy W, which is shifted into the droplet in time t, and the slope between W and t is defined as $P_{adsorpt}$. In order to make a precise prediction, the exponential function in Equation 13 is used, through which $P_{adsorpt}$ is increased step by step with the accumulation of propagation distance x. The variable Σx is used to present the accumulation amount of x in Equation 13. Inside the fully enclosed wetting environment, energy loss is generated and accounted into droplet's accumulation of energy, here $P_{adsorpt}$ is defined as the adsorption power, also being the average W shifting into the droplet in a unit time t, for predicting $P_{adsorpt}$, an exponential function is used in Equation 13, $P_{adsorpt}$ is increased step by step with the accumulation of propagation distance x, the latter is a variable which Equation 13 uses Σx to represent. Attenuation coefficient α of f=20 kHz ultrasound is predicted in an empirical equation as Equation 14, which includes viscosity η_{liquid}[41].

$$P_{adsorpt} = [p_{liquid}^2 A_{inteface} / (\rho_{liquid} c_{liqud})] \cdot [1 - exp(-2\alpha\Sigma x)] \quad (13)$$

$$\alpha = {8\pi f^2 \eta_l}\Big/{3\rho_l c_l^3} \quad (14)$$

Propagation length is assumed as the distance ultrasound wave totally travels, so it is assumed that there should be ft cycles in ultrasonic time t, so Σx equals to $fa_{solid/rms} \cdot t$ in the process of attenuation, W is calculated in Equation 15.

$$W = [2(\rho_{liquid} c_{liqud})^{-1} \alpha p_l^2 fa_{solid/rms} \cdot t] A_{interface} (\lim_{x \to 0} \frac{1-e^{-x}}{-x} = 1,\ 2\alpha\Sigma x \to 0) \quad (15)$$

Differences in internal energy ΔU would be composed of mechanical energy increment and change in surface energy $\Delta U_{surface}$ in spreading. The surface energy of droplet meets Equation 16, which is a time-dependent energy item with changing CA and surface area $A_{surface}$.

$$U_{surface} = \gamma_{lv} A_{surface} cos\theta \quad (16)$$

Therefore, a thermodynamic equation for the calculation of the internal energy differences is the next (Equation 17).

$$\triangle U = \gamma_{lv} A_{surface} cos\theta + E_k \quad (17)$$

3.4. Contact angle evaluations for curve-fitting

According to former morphological investigations, the depinning contact lines are among some partial oscillation periods but not all of them. Within several adjacent swaying cycles, the wetted diameter remains constant, either because the temporal energy values fail to change droplet shapes with various energy states in different stages, or the pinning/depinning contact lines are in dynamic balance. In general, during ultrasonic excitation with the ultrasonic work increasement, there is an overall tendency of solder spreading[42].

The velocity of spreading deeply relates with the droplet movement in the nearby cyclic period. Aforementioned studies on spreading behaviors with swaying mode indicate that droplet centroid varies with the horizontal velocity, when

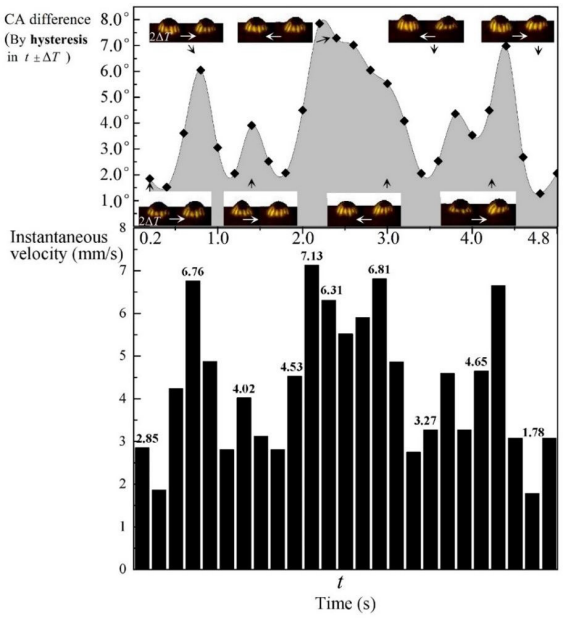

Figure 9. The level of CA hysteresis within a nearby interval ΔT of specific equilibrium wetting moments and the chart of instantaneous droplet velocity varying among wetting moments.

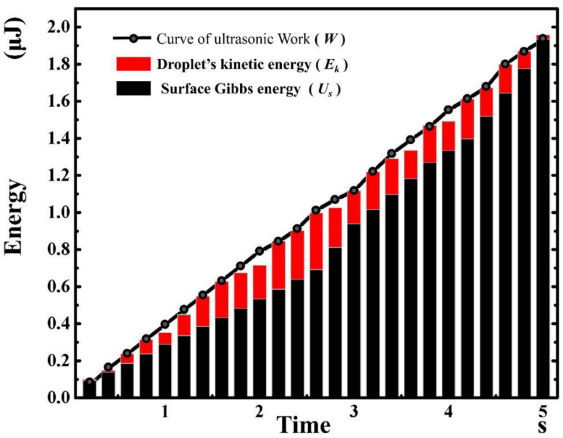

Figure 10. A fitting chart for the calculated items, surface energy $U_{surface}$ and kinetic E_k of Al droplet are depicted by black, red columns, along with the W-t variation described by the curve.

shifting leftwards or rightwards. Velocity is calculated via single point displacement method. For each droplet velocity in an equilibrium state, a 0.9 ms fragment prior to that moment, and another one after together comprises an interval ΔT (ΔT = 1.8 ms). The moving distance of centroid is measured from a screenshot sequence neighboring each equilibrium wetting moment. Instantaneous velocities at 25 moments are measured in this way, and their variation trend is showed in Figure 9. It can be deduced that CA hysteresis dominates the velocity changes, since differences and velocities own the same trend during the ultrasonic period. Instantaneous velocity of droplet rise up to maximum at an intermediate time period, while minimum velocity appear at 4.8 s when ultrasonic excitation have already stopped.

As shown in Figure 10, the curve-fitting indicates that laws of thermodynamics can be well applied to the actual ultrasonic wetting process of Al/SiC. Under the circumstance, theoretical derivations are reasonable, and Equation 10 is similarly verified with experimental results.

5. Conclusion

At 900°C, the spreading behavior of Al/SiC system in an ultrasonic-assisted wetting field differs from usual ways of spreading significantly. The swaying mode and equilibrium mode are two typical ultrasonic-assisted wetting characteristics, distinguished by exhibitions of contact angle hysteresis or not. The equilibrium wetting mode is responsible for the decreasement in contact angle, it also demonstrates an enhancement in Al/SiC wettability in timed ultrasonic period. Except that, the droplet is found to sway cyclically on substrate during 5 s exciting period. The frequency of each swaying cycle with the droplet shape oscillation is identified as 180 ms. After investigating changes in centroid position, energy increments as well as instantaneous velocities of spreading droplets, the kinetic energy E_k, surface energy is quantitively evaluated, ultrasonic work W on the interface and apparent contact angle θ_t, and their mathematic relationships are checked with laws of thermodynamics.

Kinetic spreading in an ultrasonic-assisted process is closely related to the energy states at all instants. A swaying solder droplet is found to be with a series of unstable, asymmetric body shapes, which symbolizes droplet being drifted into metastable states under periodical oscillations. Equations from acoustic theories may be used for the quantitative analysis of the solder droplet swaying behavior. Energy input by ultrasonic is continuously accumulated so that solder droplet is capable of passing over numerous partial energy states. The wetting energy state stabilizes when equilibrium contact angle comes to minimum. All measured equilibrium angles fit the proposed theoretical equation, and the θ_t-t variation can also be indicated by this equation.

6. Acknowledgement

This work was supported by the National Natural Science Foundation of China (51435004).

7. References

1. Sikalo S, Wilhelm HD, Roisman IV, Jakirlic S, Tropea C. Dynamic contact angle of spreading droplets: experiments and simulations. Phys Fluids. 2005;17:062103.
2. Sprittles JE. Kinetic effects in dynamic wetting. Phys Fluids. 2017;118:114502.
3. Zhang HY, Lai H, Cheng ZJ, Zhang D, Liu P, Li Y, et al. In-situ switchable superhydrophobic shape memory microstructure patterns with reversible wettability and adhesion. Appl Surf Sci. 2020;525(30):146525.
4. Huang S, Song J, Lu Y, Chen F, Zheng H, Yang X, et al. Underwater spontaneous pumpless transportation of nonpolar organic liquids on extreme wettability patterns. ACS Appl Mater Interfaces. 2016;8(5):2942-9.
5. Garrod RP, Harris LG, Schofield WCE, McGettrick J, Ward LJ, Teare DOH, et al. Mimicking a stenocara beetle's back for microcondensation using plasmachemical patterned

superhydrophobic-superhydrophilic surfaces. Langmuir. 2007;23(2):689-93.
6. Neild A, Ng TW, Sheard GJ, Powers M, Oberti S. Swirl mixing at microfluidic junctions due to low frequency side channel fluidic perturbations. Sens Actuators B Chem. 2010;150(2):811-8.
7. Gao XB, Li YX. Ultra-fast AC electro-osmotic micropump with arrays of asymmetric ring electrode pairs in 3D cylindrical microchannel. J Appl Phys. 2018;123(16):164301.
8. Guttenberg Z, Muller H, Habermuller H, Geisbauer A, Pipper J, Felbel J, et al. Planar chip device for PCR and hybridization with surface acoustic wave pump. Lab Chip. 2005;5(3):308.
9. Riaud A, Baudoin M, Bou Matar O, Thomas J-L, Brunet P. On the influence of viscosity and caustics on acoustic streaming in sessile droplets: an experimental and a numerical study with a cost-effective method. J Fluid Mech. 2017;821:384-420.
10. Aamir M, Muhammad R, Tolouei-Rad M, Giasin K, Silberschmidt VV. A review: microstructure and properties of tin-silver-copper lead-free solder series for the applications of electronics. Solder Surf Mt Technol. 2019;32(2):115-26.
11. Santos C, Ribeiro S, Strecker K, Rodrigues D Jr, Silva CRM. Highly dense Si_3N_4 crucibles used for Al casting: an investigation of the aluminium-ceramic interface at high temperatures. J Mater Process Technol. 2007;184(1-3):108-14.
12. Bao S, Syvertsen S, Kvithyld MA, Engh T. Wetting behavior of aluminium and filtration with Al_2O_3 and SiC ceramic foam filters. Trans Nonferrous Met Soc China. 2014;24(12):3922-8.
13. Laurent V, Chatain M, Eustathopoulos N. Wettability of SiO_2 and oxidized SiC by aluminium. Mater Sci Eng A. 1991;135(30):89-94.
14. Strani M, Sabetta F. Free vibrations of a drop in partial contact with a solid support. J Fluid Mech. 1984;141:233-47.
15. Zhou J, Xu RW, Jiao H, Bao J, Liu Q, Long Y. Study on the mechanism of ultrasonic-assisted water confined laser micromachining of silicon. Opt Lasers Eng. 2020;132:106118.
16. Yang Y, Li SR, Liang YX, Li B. The wetting phenomenon and precursor film characteristics of Sn-37Pb/Cu under ultrasonic fields. Mater Lett. 2019;234:92-5.
17. Orlova EG, Feoktistov DV, Kuznetsov GV, Ponomarev KO. Spreading of a distilled water droplet over polished and laser-treated aluminum surfaces. Eur J Mech BFluids. 2018;68:118-27.
18. Xu ZW, Ma L, Yan JC, Yang S, Du S. Wetting and oxidation during ultrasonic soldering of an alumina reinforced aluminum-copper-magnesium (2024 Al) matrix composite. Compos, Part A Appl Sci Manuf. 2012;43(3):407-14.
19. Zhu Y, Qu P, Kang H. Effects of mechanical oscillation on wettability of brazing filler metals. J Mater Eng. 1999;6:30-2.
20. Xu ZW, Yan JC, Zhong L, Yang S. Filling and wetting behaviors of liquid filler metal in the process of ultrasonic soldering of aluminum alloy. J. Mater. Eng. 2010;6:1-8.
21. Feng JC, Liu HJ, Naka M, et al. Reaction products and growth kinetics during diffusion bonding of SiC ceramic to Ni-Cr alloy. Mater. Sci. Tech-lond. 2003;19:137-42.
22. Xia YH, Wang Y, Yang ZW, Wang DP. Contact-reactive brazing of Ti_3SiC_2 ceramic to TC4 alloy using a Ni interlayer: interfacial microstructure and joining properties. Ceram Int. 2018;44(10):11869-77.
23. Lu Y, Sun GF, Wang ZD, Zhang Y, Su B, Feng A, et al. Effects of electromagnetic field on the laser direct metal deposition of austenitic stainless steel. Opt Laser Technol. 2019;119:105586.
24. Lin JL, Lee GB, Chang YH, Lien K-Y. Model description of contact angles in electrowetting on dielectric layers. Langmuir. 2006;22(1):484-9.
25. Orejon D, Sefiane K, Shanahan M. Young-Lippmann equation revisited for nano-suspensions. Appl Phys Lett. 2013;102(20):201601.
26. Yeo L, Chang HC. Electrowetting films on parallel line electrodes. Phys Rev E Stat Nonlin Soft Matter Phys. 2006;011601:73.
27. Vukasinovic B, Smith MK, Glezer A. Dynamics of a sessile drop in forced vibration. J Fluid Mech. 2007;587:395-423.
28. Benilov ES, Cummins CP. Thick drops on a slowly oscillating substrate. Phys Rev E Stat Nonlin Soft Matter Phys. 2013;88(2):023013.
29. Daniel S, Chaudhury MK, De Gennes PG. Vibration-actuated drop motion on surfaces for batch microfluidic processes. Langmuir. 2005;21(9):4240-8.
30. Whitehill JD, Neild A, Wah TN, Martyn S, Chong J. Droplet spreading using low frequency vibration. Appl Phys Lett. 2011;13350:2198.
31. Whitehill JD, Neild A, Stokes MH. Forced spreading behavior of droplets undergoing low frequency vibration. Colloids Surf A Physicochem Eng Asp. 2012;393:144-52.
32. Scortesse J, Manceau JF, Bastien F. Interaction between a liquid layer and vibrating plates: application to the displacement of liquid droplets. J Sound Vibrat. 2002;254(5):927-38.
33. Ekere NN, He D, Riedlin MA. The viscoelastic characteristics of solder paste under high frequency oscillatory shear. In: Twenty Third IEEE/CPMT International Electronics Manufacturing Technology Symposium; 1998; Austin, TX, USA. New York: IEEE; 1998. p. 373-6.
34. Faridi HR, Devletian JH, Le HP. A new look at flux-free ultrasonic soldering. Vibrations. 2000;79:41-5.
35. Lanin VL. Ultrasonic soldering in electronics. Ultrason Sonochem. 2001;8(4):379-85.
36. Saxty P. Ultrasonic soldering-a farewell to flux. Weld Met Fabr. 1999;67:15-7.
37. Aziz SD, Chandra S. Impact, recoil and splashing of molten metal droplets. Int J Heat Mass Transf. 2000;43(16):2841-57.
38. Perlin M, Schultz WW, Liu Z. High Reynolds number oscillating contact lines. Wave Motion. 1999;67:1.
39. Shi L-X, Shen P, Zhang D, Jiang Q-C. Wetting and evaporation behaviors of molten Mg–Al alloy drops on partially oxidized α-SiC substrates. Mater Chem Phys. 2011;130(3):1125-33.
40. Ma L, Xu ZW, Zheng K, Yan J, Yang S. Vibration characteristics of Aluminum surface subjected to ultrasonic waves and their effect on wetting behavior of solder droplets. Ultrasonics. 2014;54(3):929.
41. Chu HY, Chen JK. Evolution of viscosity of concrete under sulfate attack. Constr Build Mater. 2013;39:46-50.
42. Miyamoto K, Nagatomo S, Matsui Y, Shiokawa S. Nonlinear vibration of liquid droplet by surface acoustic wave excitation. Jpn J Appl Phys. 2002;41(Part 1, No. 5B):3465-8.